


Advanced fiber in-coupling through nanoprinted axially symmetric structures

Cite as: Appl. Phys. Rev. **10**, 011401 (2023); <https://doi.org/10.1063/5.0127370>

Submitted: 21 September 2022 • Accepted: 15 December 2022 • Published Online: 03 January 2023

 Oleh Yermakov,  Matthias Zeisberger,  Henrik Schneidewind, et al.

COLLECTIONS

 This paper was selected as Featured



View Online



Export Citation



CrossMark

ARTICLES YOU MAY BE INTERESTED IN

[Liquid metal gallium-based printing of Cu-doped p-type Ga₂O₃ semiconductor and Ga₂O₃ homojunction diodes](#)

Applied Physics Reviews **10**, 011402 (2023); <https://doi.org/10.1063/5.0097346>

[Tripling energy storage density through order-disorder transition induced polar nanoregions in PbZrO₃ thin films by ion implantation](#)

Applied Physics Reviews **10**, 011403 (2023); <https://doi.org/10.1063/5.0102882>

[Optical manipulation with metamaterial structures](#)

Applied Physics Reviews **9**, 031303 (2022); <https://doi.org/10.1063/5.0091280>



Applied Physics Reviews

Special Topic: Materials and Technologies
for Bioimaging and Biosensing

Submit Today!

Advanced fiber in-coupling through nanoprinted axially symmetric structures

Cite as: Appl. Phys. Rev. **10**, 011401 (2023); doi: [10.1063/5.0127370](https://doi.org/10.1063/5.0127370)

Submitted: 21 September 2022 · Accepted: 15 December 2022 ·

Published Online: 3 January 2023










View Online



Export Citation



CrossMark

Oleh Yermakov,^{1,a)}  Matthias Zeisberger,²  Henrik Schneidewind,²  Jisoo Kim,²  Andrey Bogdanov,³ 
Yuri Kivshar,⁴  and Markus A. Schmidt^{2,5,6,a)} 

AFFILIATIONS

¹V. N. Karazin Kharkiv National University, Kharkiv 61022, Ukraine

²Leibniz Institute of Photonic Technology, Jena 07745, Germany

³Harbin Engineering University, Harbin 150001, China

⁴Nonlinear Physics Centre, Research School of Physics, Australian National University, Canberra ACT 2601, Australia

⁵Abbe Center of Photonics and Faculty of Physics, Friedrich-Schiller-University Jena, Jena 07743, Germany

⁶Otto Schott Institute of Material Research, Jena 07743, Germany

^{a)} Authors to whom correspondence should be addressed: oe.yermakov@gmail.com and markus.schmidt@leibniz-ipht.de

ABSTRACT

Here, we introduce and demonstrate nanoprinted all-dielectric nanostructures located on fiber end faces as a novel concept for the efficient coupling of light into optical fibers, especially at multiple incidence angles and across large angular intervals. Taking advantage of the unique properties of the nanoprinting technology, such as flexibly varying the width, height, and gap distance of each individual element, we realize different polymeric axial-symmetric structures, such as double-pitch gratings and aperiodic arrays, placed on the facet of commercial step-index fibers. Of particular note is the aperiodic geometry, enabling an unprecedentedly high average coupling efficiency across the entire angular range up to 80°, outperforming regular gratings and especially bare fibers by orders of magnitude. The excellent agreement between simulation and experiment clearly demonstrates the quality of the fabricated structures and the high accuracy of the nanoprinting process. Our approach enables realizing highly integrated and ready-to-use fiber devices, defining a new class of compact, flexible, and practically relevant all-fiber devices beyond the state-of-art. Applications can be found in a variety of cutting-edge fields that require highly efficient light collection over selected angular intervals, such as endoscopy or quantum technologies. Furthermore, fiber functionalization through nanoprinting represents a promising approach for interfacing highly complex functional photonic structures with optical fibers.

© 2023 Author(s). All article content, except where otherwise noted, is licensed under a Creative Commons Attribution (CC BY) license (<http://creativecommons.org/licenses/by/4.0/>). <https://doi.org/10.1063/5.0127370>

I. INTRODUCTION

Optical fibers are key photonic devices of modern photonics and have been successfully applied in a variety of fields, including telecommunication and life science. By far, the most successful geometry commonly used is a step-index fiber made of silica with a doped core that supports one optical mode [single-mode fiber (SMF)].

Due to flexible and robust light transportation, SMFs principally represent ideal candidates for applications that demand to remotely collect light and reproducibly transport it to a predefined location. While the actual light transport capabilities are excellent, the main problem arises at the beginning of the fiber where the light is to be collected. Here, the disadvantage of commercial SMFs is the low refractive index contrast between core and cladding, imposing low numerical apertures, with the consequence that light can only

efficiently be collected for angles close to the fiber axis. For example, the most widely used SMF (Corning SMF-28¹) allows efficient modal excitation only up to a maximum angle of incidence of 25° [see the inset in Fig. 3(b)]. This drawback has hindered their use in fields that require efficient light collection, such as quantum technology or *in-vivo* endoscopy. Increasing the numerical aperture through higher index contrasts has practical limitations and leads to fibers that are incompatible with fiber optics circuitry.

One solution is the functionalization of fiber end faces with nanostructures, representing a sharply growing research field due to unique opportunities for both basic science and application. A selection of achievements of this field, sometimes referred to as “lab-on-fiber,”^{2–5} includes metalens-based device and diffractive optical elements for light focusing,^{6–8} light conversion,^{9,10} optical trapping,¹¹ holography,¹² and

plasmonic structures or arrays of nanoelements for surface-enhanced spectroscopy and sensing.^{4,13,14}

The first successful experiments on boosting coupling efficiencies at selected angles of incidence through fiber-interfaced nanostructures used arrays of plasmonic nanodots located on SMF-28.^{15,16} This arrangement enhances the coupling efficiencies up to angles of 80° through opening an additional diffraction channel, outperforming the original SMFs by orders of magnitude. The obtained results were substantially improved in terms of coupling efficiency in a recent experiment with all-dielectric nanostructures consisting of concentric rings made from SiN, achieving percentage levels of in-coupling efficiency at almost grazing angles of incidence (~80°).¹⁷ In contrast to plasmonic materials, dielectric nanostructures are highly suitable for fiber applications due to their operation in transmission and negligible absorption.^{18,19} Even though nanostructure-empowered fiber in-coupling was successfully demonstrated, the restriction to single selected angles using single-pitch arrays is unfavorable for many applications, thus requiring a substantial extension of the approach.

Due to the challenges of nanostructure fabrication on fiber, such as extremely large aspect ratio and the proper centering requirement, the choice of manufacturing process is crucial. In addition to self-assembly,^{10,20,21} electron- and ion-beam lithography,^{14,17,22–24} 3D nanoprinting by direct laser writing has boosted this research field. This technology offers decisive advantages regarding the functionalization of fiber surfaces, such as speed, ease of handling, high success rate and direct application of the devices after nanostructure implementation. Examples of nanoprinted structures on fibers include microlenses,^{25–29} photonic crystals,²⁵ achromatic⁸ and diffractive^{11,12,30} metalenses for focusing,^{8,30} beam shaping,^{25,26} imaging,²⁷ optical trapping,¹¹ polarization conversion,²⁵ vortex generation,²⁸ holography,¹² and endoscopy.²⁹ The presented considerations, therefore, suggest that the use of nanostructures on fibers includes a significant practical application potential for efficient and fiber-integrated light collection with properties tailored to the specific application, which represents the motivation for this study.

In this work, we demonstrate, for the first time, that nanoprinted structures on fiber end faces can uniquely be used for tailored and highly efficient coupling of light into the supported mode of SMF at multiple selected angles or over wide angular intervals [Fig. 1(a)]. Crucial to this concept is the use of nanoprinted polymer elements, having significant advantages over other methods and thus allowing to go beyond single-pitch arrays. A variety of otherwise difficult-to-implement geometries has been fabricated, including axially symmetric grids with double periodicity and aperiodic lattice that uniquely incorporate variation in the width and height of the elements as well as their spacing. While the former allows light coupling at multiple predefined angles with the same nanostructure, the aperiodicity (different pitch, width and height) of the latter results in an unprecedentedly high average coupling efficiency that is almost independent of the angle of incidence. Clear manufacturing and design strategies based on simulations and theoretical considerations are presented, which allow a design to be found for any practical application on demand.

II. DESIGN AND DEFINITIONS

A. Nanostructure-on-fiber designs

For all scientific findings presented here, the SMF-28 is considered as fiber platform. This single-mode fiber (HE₁₁-mode) has a core and outer diameter of 8.2 and 125 μm, with corresponding refractive

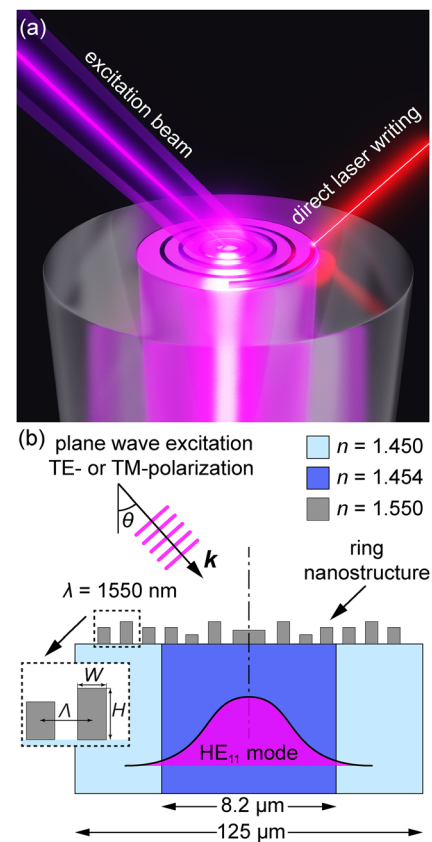


FIG. 1. (a) Artistic illustration of light coupling in optical fibers through axially symmetric nanostructures fabricated by direct laser writing. (b) Schematic cross section view of the light in-coupling problem. The incident light reaches the end face of the single-mode fiber (SMF-28) under an angle θ [core (cladding) refractive index and diameter: $n = 1.454$ ($n = 1.450$) and $d = 8.2 \mu\text{m}$ ($d = 125 \mu\text{m}$), respectively]. The supported fundamental fiber mode (HE₁₁-mode) is efficiently excited by the axial-symmetric polymeric ($n = 1.550$) nanostructures. The inset shows the geometric dimensions of two adjacent concentric rings (width W and height H) and their center-to-center distance (pitch Λ).

indices of core and cladding of 1.454 and 1.450 (at operational wavelength $\lambda = 1550 \text{ nm}$), respectively.

The nanostructures used here are arrays of axial-symmetric concentric rings made of a polymer with a refractive index $n_p = 1.55$ (see Sec. VB for details). The center of the structure is aligned with the fiber axis. The individual ring is defined by the respective ring width W and height H [see Fig. 1(b)]. The lattice itself contains a disk of diameter W_0 in the center and is determined by the center-to-center pitch Λ . It should be mentioned again that due to the unique properties of the 3D nanoprinting process, each ring can have an individual height and width in contrast to structure implemented through common lithographic approaches. Selected examples of the fabricated nanoring arrays on fiber tips are shown in Fig. 2.

B. Definition of key parameters

The essential aspect of this study is to investigate the coupling efficiency as a function of the incident angle θ for different

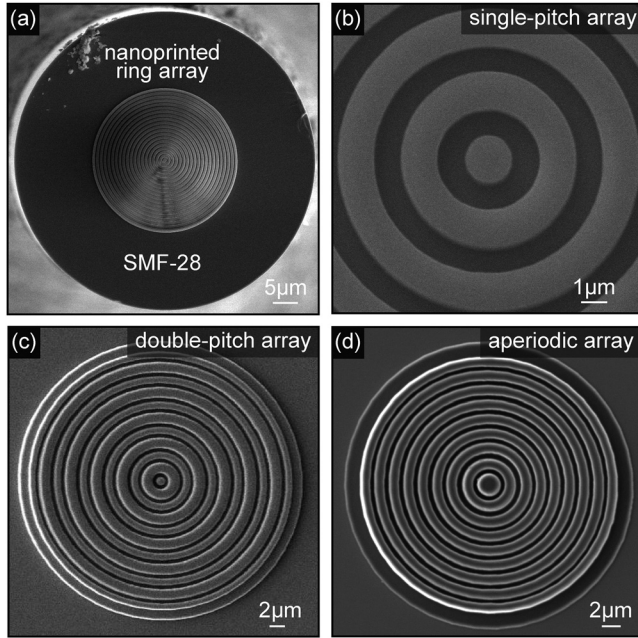


FIG. 2. Selected SEM images of axially symmetric polymer-based nanostructures located on the end faces of optical fibers (SMF-28), implemented through employing 3D nanoprining: (a) Overview of a fiber end face on which a nanostructure has been nanoprined. The remaining images show implemented examples of the geometries that were studied in this work; (b) single-pitch ring array; (c) double-pitch ring array; and (d) aperiodic axial-symmetric nanostructure.

nanostructures at the operational wavelength λ . This value indicates the efficiency with which the power of the plane wave incident on the fiber end face under an angle θ is transferred to the guided fiber mode. Since the definition of this essential parameter is inconsistently reported in the literature, the definitions relevant for this work are introduced in the following in detail, to allow for a direct comparison to reported values. Note that since the SMF-28 is used exclusively as the fiber platform, the operation wavelength is chosen to be in the single-mode regime of this fiber type, which is the wavelength of the probe light used in the experiment.

1. Effective coupling-area-related efficiency

The first parameter to be introduced is the coupling-area-related efficiency $\eta_0(\theta)$, which is the ratio of the effective coupling area A_c to the area of the mode inside the fiber A_m ,

$$\eta_0(\theta) = \frac{A_c(\theta)}{A_m}. \quad (1)$$

According to the specification of the SMF-28 fiber (Corning data-sheet¹), the mode diameter is $10.5 \mu\text{m}$, resulting in a mode area of $A_m = 86.6 \mu\text{m}^2$. The effective coupling area is an essential parameter since it can be directly obtained from the measurements. Experimentally, A_c is defined as the ratio of the measured guided-mode power $P_{\text{out}}(\theta)$ to the intensity of the incident light I_0 , yielding $A_c(\theta) = P_{\text{out}}(\theta)/I_0$. Further details on the evaluation of this parameter can be found in Sec. V C.

2. Normalized fiber in-coupling efficiency

To allow for a direct comparison of the experimental data and simulations and to benchmark the results, we introduce the normalized in-coupling efficiency, which is defined as the ratio of coupling-area-related coefficient (or effective coupling area) at angle θ to its counterpart for bare fiber at normal incidence ($\theta = 0^\circ$),

$$\eta_n(\theta) = \frac{\eta_0(\theta)}{\eta_0^{\text{bare}}(\theta = 0)} = \frac{P(\theta)}{P^{\text{bare}}(\theta = 0)}. \quad (2)$$

This definition is useful in the context of this work, since the highest possible value of coupling efficiency is achieved by a bare fiber at normal light incidence [$\max(\eta_0^{\text{bare}}) = \eta_0^{\text{bare}}(\theta = 0)$], thus representing the maximum possible benchmark value for this type of fiber. Any kind of surface nanostructure on the fiber leads to additional reflection, thus reducing the in-coupling efficiency. Another practical advantage of using the normalized coupling efficiency is its independence from the intensity of the incident light.

3. Average fiber in-coupling efficiency

In case the incident light contains an ensemble of plane waves at different angles rather than a single wave, it is convenient to use the average coupling efficiency as a benchmark figure,

$$\overline{\eta}_n(\theta_1, \theta_2) = \frac{\int_{\theta_1}^{\theta_2} \eta_n(\theta) d\theta}{\theta_2 - \theta_1}. \quad (3)$$

This value shows the average value of normalized in-coupling efficiency within an angle interval $\theta_1 < \theta < \theta_2$.

4. Boosting factor for nanostructured fiber

To quantify the enhancement of the in-coupling efficiency for the nanostructured fiber at a selected angle in comparison with a bare fiber, the boosting factor is introduced as follows:

$$\text{BF} = \frac{\eta(\theta)}{\eta^{\text{bare}}(\theta)} = \frac{P(\theta)}{P^{\text{bare}}(\theta)}. \quad (4)$$

All fiber coupling efficiencies presented are dimensionless and have a concrete physical meaning in the context of the measurements.

III. RESULTS AND DISCUSSION

To show all relevant features of the nanoprined structures regarding fiber in-coupling, different types of the described concentric geometry have been implemented. First, three different periodic arrangements of identical rings are investigated, each showing local maxima of in-coupling efficiency at a preselected angle. Furthermore, double-pitch arrangements with two types of rings were characterized, yielding two local maxima at different angles. The highest structural complexity was reached by an aperiodic array, in which all rings (also in height of the individual element) and their mutual arrangement are different. This structure yields a high average in-coupling efficiency over the entire angular range from 0° to 85° . Finally, the normalized and average coupling efficiencies for all these nanorings are compared.

For the experimental realization of the on-fiber dielectric nanostructures, direct laser writing using a commercial nanopriner

(Photonic Professional GT2, Nanoscribe GmbH³¹) was applied to the surface of SMF-28 (further details can be found in Sec. VB). As previously mentioned, this type of technology is already successfully used in multiple fiber-related applications and results in samples that can be directly applied after structure implementation.^{12,29} High-resolution scanning electron micrograph (SEM) and atomic force microscopy (AFM) imaging have been used to characterize a representative sample. The optical characterization relies on a combination of light sources and the sample,²⁴ which can be aligned at a defined angle to each other, and a detector unit. Details about the setup and the measurement procedure method can be found in Sec. VC. The details on numerical simulation approach based on finite-element method could be found in Sec. VA.

A. Single-pitch nanostructure

In the first step, regular periodic arrays of concentric polymer rings with different pitches, located on SMF-28, are investigated. This study serves as a proof-of-concept that the diffraction-based in-coupling approach introduced in Refs. 15 and 17 is also applicable in the case of polymer structures. Note that the crucial difference here is the lower refractive index of the polymer structures in contrast to the high-index refractive structures used in Ref. 17. For one geometry, all rings have the same geometric parameters with constant pitch and the central element being a disk. All geometric parameters are shown in Table I. By using the lattice resonance condition of a linear one-dimensional grating $\theta_{\text{res}} = \arcsin(\lambda/\Lambda)$ as an initial approach for estimating the local maximum angle (given in Refs. 15 and 17) the geometric parameters of three designs were further numerically optimized (see Sec. VA) to achieve maximal in-coupling efficiencies at 40°, 60°, and 75°. As discussed in Refs. 15 and 17, the observed maxima arise from the minus first-order diffraction channel. For the optimization, we first use an analytical approach presented in our previous work¹⁷ to select a proper pitch of the structure according to the angle of interest, and proper width and height of the rings to maximize the normalized

TABLE I. Geometric parameters and measured normalized in-coupling efficiencies at local maxima of three different nanostructures (NS) consisting of single-pitch periodic polymer rings. Note that the parameters of the central disk differs from the rings and is characterized by the diameter W_0 and the distance to the center of the first adjacent ring Λ_0 .

Geometric parameters	NS no. 1	NS no. 2	NS no. 3
Pitch (Λ), μm	2.42	1.78	1.54
Ring width ($W = 0.5 \Lambda$), μm	1.21	0.89	0.77
Ring height ($H = 0.8 \Lambda$), μm	1.94	1.42	1.23
Diameter of central disk ($W_0 = W + 0.5$), μm	1.71	1.39	1.27
Distance from origin to center of first ring ($\Lambda_0 = \Lambda + 0.25$), μm	2.67	2.03	1.79
Rings number (N_r)	13	20	20
Measured local max (η_n)			
Local maximum, °	40	60	75
TM polarization	1.9×10^{-2}	1.8×10^{-3}	1.7×10^{-4}
TE polarization	1.7×10^{-2}	1.3×10^{-3}	0.8×10^{-4}

in-coupling efficiency η_n in the vicinity of the local maximum. Finally, we numerically optimize the geometric parameters of the central disk and specify all the parameters. Note that using a larger number of rings leads to a more uniform angular distribution of the coupling efficiency since the modulations caused by additional local maxima of the diffraction are suppressed.¹⁷ Figure 3 shows the distribution of the normalized in-coupling efficiency [Eq. (2)] as a function of the incident angle θ , calculated numerically (colored dashed lines) and measured experimentally (colored solid lines). It is evident that all features of the in-coupling efficiency distribution, including the finely structured peaks and dips, correspond well between simulated and

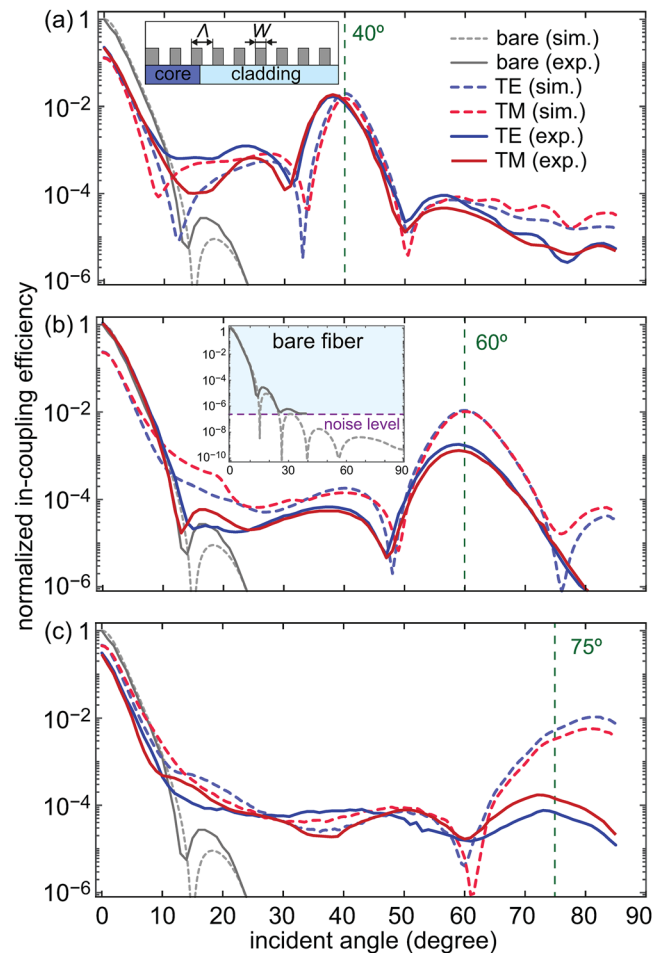


FIG. 3. Single-pitch nanostructure. Dependence of the normalized in-coupling efficiency η_n on the angle of incidence for the interval $0^\circ < \theta < 85^\circ$ for three different single-pitch nanostructure designs optimized to exhibit a respective local in-coupling maximum at a preselected angle [vertical dashed green lines] (a) $\theta = 40^\circ$, (b) $\theta = 60^\circ$, and (c) $\theta = 75^\circ$. The dashed and solid lines correspond to the simulated and experimental results, while the blue and red lines refer to the TE- and TM-polarization, respectively. The gray lines in each plot show the in-coupling efficiency for a bare fiber without nanostructure. The inset in (b) shows the in-coupling efficiency of the bare fiber, including the experimental noise limit ($\eta_0 \approx 2 \times 10^{-7}$, experimentally accessible domain is indicated by the light blue area).

measured data. At large angles ($\theta > 70^\circ$), the measured coupling efficiency is much lower than its counterpart in the plane wave-based simulation as the intensity of the Gaussian beam transmission sharply drops in case θ reaches values larger than 70° .³² The reason for the difference in local maximum angle θ_{res} between full numerical simulations and experimental results at 75° is associated mainly with the strong dependence of η_n on Λ in the case of large incident angles θ (more details can be found in the [supplementary material](#)). It is remarkable that the coupling efficiencies of the fibers with nanostructured tips exceed the performance of the bare fibers (gray lines) by several orders of magnitude across large angle intervals. Note that for $\theta > 23^\circ$, coupling into bare fibers is hardly possible ($\eta_n < 10^{-6}$), while the nanostructured-empowered fibers show significant coupling, particular at the preselected angles. We would like to mention that the experimental noise level is roughly $\eta_n \approx 2 \times 10^{-7}$. Thus, in the case of the bare fiber, no values can be measured for $\theta > 40^\circ$ [inset in Fig. 3(b)], whereas for the nanostructure-empowered fiber a value can be determined for all angles relevant here.

The measured value of the normalized in-coupling efficiency η_n at the angle the respective local maxima occurs are 1.9×10^{-2} (1.7×10^{-2}), 1.8×10^{-3} (1.3×10^{-3}), and 1.7×10^{-4} (0.8×10^{-4}) for TM (TE) polarization at $\theta = 40^\circ$, 60° , and 75° , respectively. Note that the achieved magnitudes of in-coupling efficiency and measured curve shapes correspond to those determined for high-index structures reported in the previous work.¹⁷ This observation clearly highlights that nanoprinted polymer structures are excellently suited for improving in-coupling efficiency of optical fibers and underlines the relevance of the nanoprinting process in the context of fiber functionalization. The additional peaks and dips in-between the main features correspond to the additional diffraction maxima between the 0th and -first-diffraction orders that analogously emerge in conventional diffraction gratings that have a finite number of slits.¹⁷ Here, the number and amplitudes of the additional maxima are proportional and inversely proportional to the number of the slits, respectively.³³

B. Double-pitch nanostructure

In this section, geometrically more complex nanostructures, i.e., geometries containing a quasi-periodic arrangement ($\Lambda_i = 1.8 \mu\text{m}$), on SMF-28 are analyzed. The geometry considered consists of two different types of ring arrays, arranged in alternating sequence [inset in Fig. 4(a)]. The two types of rings differ in all geometrical parameters (details in Table II). The main idea is to simultaneously achieve high in-coupling efficiency at two well-separated angles. The measurements show two distinct local maxima at $\theta = 25^\circ$ and $\theta = 60^\circ$, with the experimental results being very well reproduced by the numerical results. It is worth highlighting the excellent agreement at the two angles of maximal coupling efficiency for both polarization directions, which underlines the quality of the fabricated nanostructures and the high accuracy of the nanoprinting process itself. The measured value of the normalized in-coupling efficiency η_n at the angle the local maxima in the vicinity of 25° and 60° are 9.2×10^{-3} (7.9×10^{-3}) and 2.9×10^{-3} (1.9×10^{-3}) for TM (TE) polarization, respectively. It is also worth mentioning that here, for the first time, efficiencies in the percentage range could be achieved simultaneously at two different angles with only one nanostructure. High-resolution SEM and AFM images of focused ion-beam (FIB) milled sections of the grating (details in the [supplementary material](#)) were used to compare the

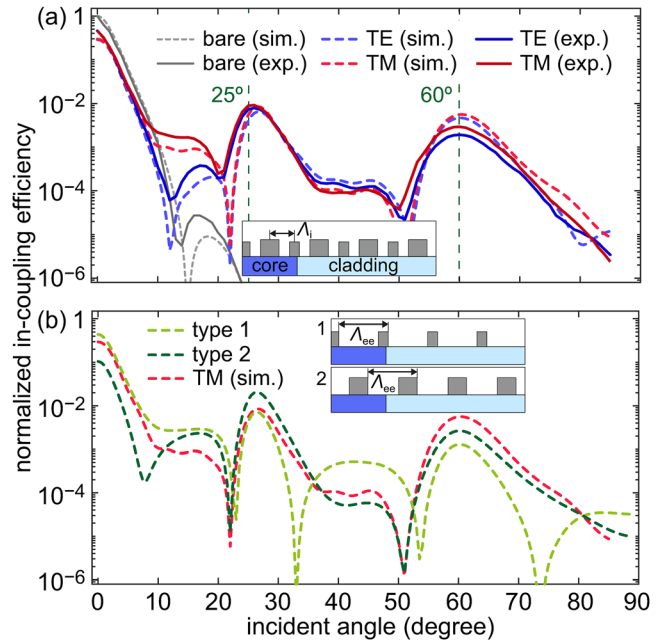


FIG. 4. Double-pitch nanostructure. Angular distribution of the normalized in-coupling efficiency (from 0° to 85°) for the double-pitch ring-like nanostructure. The dashed and solid lines correspond to the simulated and experimental results, while the blue and red lines refer to the TE- and TM-polarization, respectively. The gray lines show the in-coupling efficiency for a bare fiber without nanostructure. The vertical green dashed lines refer to the preselected angles of local maxima ($\theta = 25^\circ$ and $\theta = 60^\circ$). (b) Angular distribution of the in-coupling efficiency of the individual single-pitch gratings of two types defined in Table II (types 1 and 2 correspond to dashed light and dark green lines, respectively) together with the simulated data of the double-pitch structure (dashed red line). The sketches in (a) and (b) illustrate the double-pitch and single-pitch nanostructures, respectively.

TABLE II. Geometric parameters of two types of rings and measured normalized in-coupling efficiencies at two local maxima of a double-pitch ring-like nanostructure. Note that the parameters of the central disk differs from the rings and is characterized by the diameter $W_0 = 1.02$, height $H_0 = 1.08 \mu\text{m}$ and the distance to the center of the first adjacent ring $\Lambda_0 = 1.95 \mu\text{m}$.

Geometric parameters	Ring-type no. 1	Ring-type no. 2
Element-to-element pitch (Λ_{ee}), μm	3.6	
Ring width (W), μm	0.72	1.26
Ring height (H), μm	1.08	1.35
Rings number (N_r)	5	5
Measured local max(η_n)	Double-pitch nanostructure	
Local maximum, $^\circ$	26	60
TM polarization	9.2×10^{-3}	2.9×10^{-3}
TE polarization	7.9×10^{-3}	1.9×10^{-3}

geometric parameters of the fabricated structures to the design parameters. The values for the periods as well as for the widths of the rings largely correspond to the design values. For the height of the rings, a stronger deviation from the nominal value of about 20% was found. To show a possible influence of the height deviation, the $\eta_n(\theta)$ distribution was simulated for the design and the measured structural parameters. The simulated distributions differ only very slightly, and thus, no substantial change of the measured in-coupling efficiency distribution is to be expected due to other experimental errors (see [supplementary material](#)).

For a deeper understanding of the double-pitch nanostructure and to explain the occurrence of two maxima of η_n , the angle-dependent coupling efficiency of the individual ring gratings was simulated [Fig. 4(b)]. Note that in this case, the period for each individual grating Λ_{ee} is equal to $\Lambda_{ee} = 2\Lambda_i = 3.6 \mu\text{m}$ [inset in Fig. 4(b)]. Due to the relatively large value of Λ_{ee} , two diffraction channels corresponding to two local maxima are opened. Similar to Sec. III A, this design was optimized in terms of achieving high coupling efficiency at the local maxima, corresponding to the two selected angles at the same time. Further optimization of the individual type of ring aimed at reaching approximately equal values of η_n at the two local maxima [Fig. 4(b)]. We would like to highlight again the possibility of individual height and width optimization of the two ring types, which is important to maximize the coupling efficiency according to the indicated optimization strategy.

C. Aperiodic rings

To investigate a nanostructure with a high degree of complexity, a ring lattice with an aperiodic sequence of elements is examined in Secs. III D–III F. The purpose of this structure is to couple-in an as-wide-as-possible angular spectrum at high efficiency into the SMF-28. The structure considered here consists of four types of ring-like elements (one central disk and three different grating types, details can be found in Table III). It has been optimized to achieve both the highest possible and angle-independent average coupling efficiency. The first optimization target was to achieve $\eta_n(\theta) > 10^{-4}$ for all the incident angles within the range of $20^\circ < \theta < 85^\circ$. In the next step, we maximized the average coupling efficiency [Eq. (3)] within the same angular range. In contrast to the previous structures, the optical properties of this aperiodic array can no longer be described through the lattice resonance condition [$\theta = \arcsin(\lambda/\Lambda)$], since there is no (quasi-)periodicity presented, as the rings have different spacing and geometries. Proper optimization was achieved by multiple variations of the

TABLE III. Geometric parameters of different structural elements in the aperiodic nanostructure. Here, center-to-center distance means the distance between the centers of adjacent rings. Note that the central disk center coincides with fiber axis.

Element no.	Type of element	Ring width, μm	Ring height, μm	Center-to-center distance, μm
1	Disk	1.15 (radius)	2.1	0
2	Ring	0.9	1.7	2.4
3	Ring	0.9	1.6	1.8
4–9	Ring	0.8	1.6	1.6

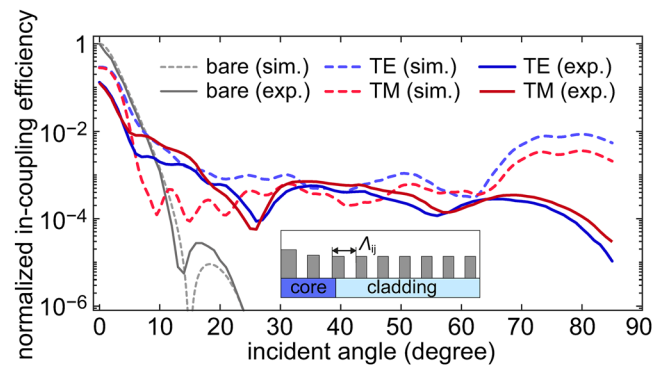


FIG. 5. Aperiodic nanostructure. Angular distribution of the normalized in-coupling efficiency ($0^\circ < \theta < 85^\circ$) for the aperiodic ring-like nanostructure (each i th element is characterized by the different width, height and distance to the neighboring j th element Λ_{ij} , see the inset). The dashed and solid lines correspond to the simulated and experimental results, while blue and red lines refer to TE- and TM-polarization. The gray lines show the in-coupling efficiency for a bare fiber without a nanostructure.

geometrical parameters of the first four rings, which are the dominant contributors to the light coupling process.

The measured data, which correspond very well to the simulated ones, clearly show, in contrast to the previous investigations, a flat distribution of the coupling efficiency (Fig. 5). Similar to the case of the single-pitch nanostructure with local maximum at 75° , the measured coupling efficiency is lower than predicted in the simulations at large incident angles, which can be attributed to the sharp decreasing of the Gaussian beam transmission.³² The measured in-coupling efficiency is $\eta_n > 10^{-4}$ over a wide range of angles up to $\theta < 80^\circ$ as shown in Fig. 6(b). As expected, in this case the structure has no defined diffraction channel, so the light in-coupling at a specified angle is not as efficient as for the strictly periodic structures. However, the average in-coupling efficiency for arbitrary angular intervals defined by (θ_1, θ_2) is higher for the aperiodic structure due to the deep optimization. This represents an outstanding feature of this structure and illustrates that well-designed nanostructures are excellent candidates for enhancing the in-coupling of light into fiber.

D. Performance comparison—normalized coupling efficiency at individual angle

In the following, the different nanostructures are compared regarding the coupling efficiency at discrete angles θ among each other and in relation to a fiber without nanostructure. An important parameter in this context is the boosting factor BF [Eq. (4)], which indicates the improvement of the coupling efficiency compared to a bare fiber at a certain angle over the entire angular spectrum relevant here ($0^\circ < \theta < 85^\circ$). It should be noted that for large angles $\theta > 40^\circ$, the coupling efficiency of the bare fiber falls below the noise level of the detector [inset in Fig. 3(b)], and thus, a constant coupling efficiency at noise level ($\eta_n = 2 \times 10^{-7}$) was assumed for the calculation of the boosting factor. Thus, the boosting factor presented in Fig. 6(a) represents a conservative estimate of the improvement for angles greater than 40° , whereas the actual boosting factor will be much higher for large angles due to the very low real coupling efficiency into the bare fibers. Overall, the improvement is clearly visible for $\theta > 15^\circ$, since from this angle the light coupling is dominated by

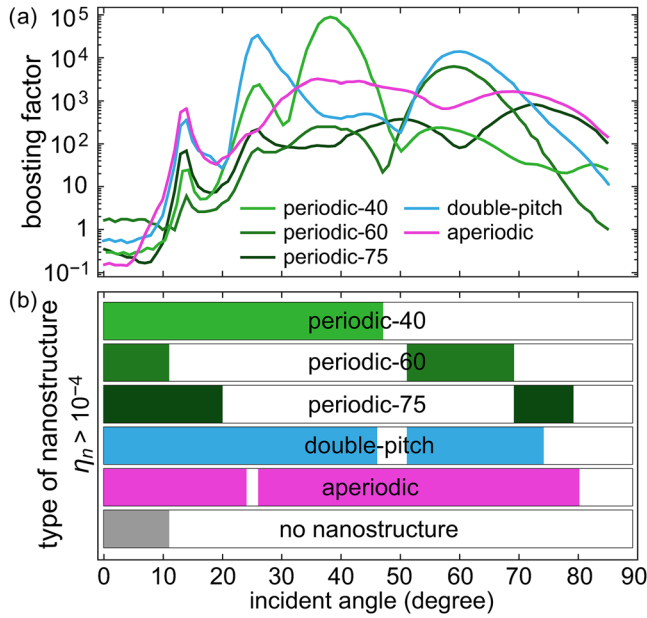


FIG. 6. Comparison of nanostructures boosting: (a) Boosting factor showing the enhancement of in-coupling efficiency compared to a bare fiber vs the angle of incidence for different polymer rings designs. Light-green, green, dark-green, blue, and magenta lines correspond to the periodic with local maxima at 40°, 60°, and 75°, double-pitch and aperiodic structures, respectively. (b) The bar chart showing the range of incident angles corresponding to the values of the normalized in-coupling efficiency $\eta_n > 10^{-4}$ for different types of nanostructured fibers under consideration.

the nanostructure. As expected, the structures with defined periodicity show very large improvements (typically, by 3–4 orders of magnitude) at certain angles, whereas the aperiodic structure shows a flat behavior over a large angular range.

For further comparing the nanostructures-enhanced fibers, the angular intervals of the different structures in which they exceed a certain value of the coupling efficiency (here $\eta_n > 10^{-4}$) were determined [Fig. 6(b)]. This comparison clearly shows that the nanostructures with higher complexity [double-pitch (blue) and aperiodic (magenta)] have much wider operating ranges than those with single pitches (green bars). Interestingly, the performance of the double-pitch structure (blue) is only slightly below that of the aperiodic structure (magenta). All fibers functionalized with nanostructures exhibit much broader regions of high coupling efficiency than the bare fiber (gray).

E. Performance comparison—average coupling efficiency

Certain applications do not demand a high coupling efficiency at a single specific angle θ , but require a high coupling efficiency across a selected angular spectrum of plane waves that incident on the fiber. As described in Sec. II B, the average coupling efficiency $\bar{\eta}_n(\theta_1, \theta_2)$ [Eq. (3)] provides a suitable benchmark value in this aspect. Here, the average coupling efficiency was determined for all geometries investigated from the experimental data and the simulation results are compared in Fig. 7. In general, the statements discussed in the context of the

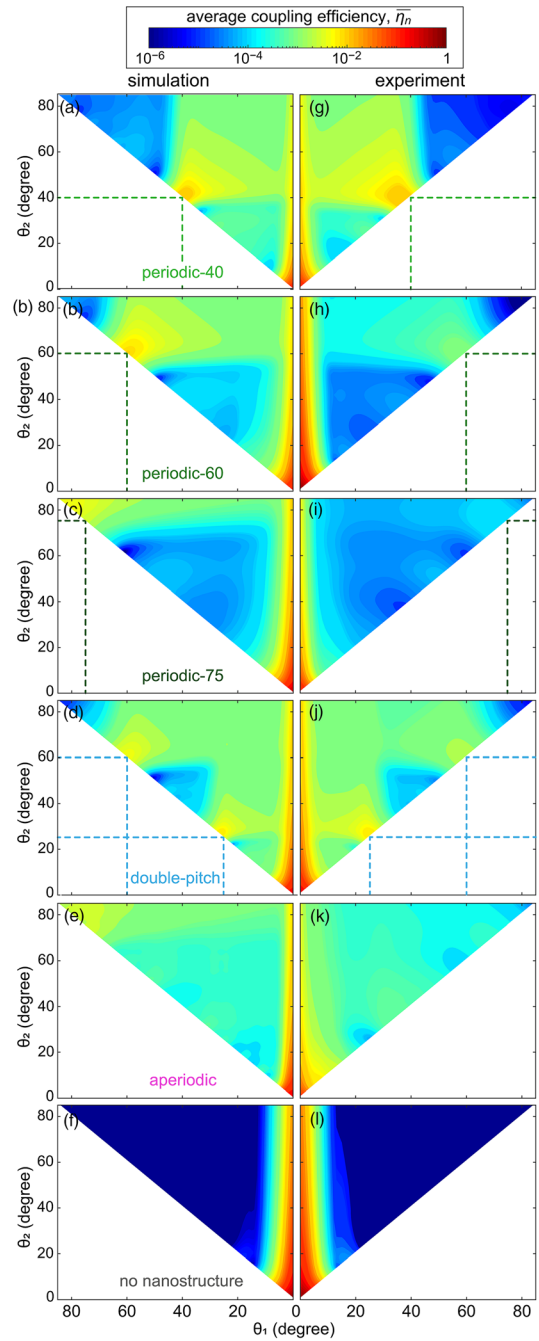


FIG. 7. Average in-coupling efficiency $\bar{\eta}_n$ [Eq. (3)] for TM polarization as a function of the angle interval (defined by the angles θ_1 and θ_2) for the different geometries investigated in this work (single-pitch nanostructures showing one local maxima at (a) and (g) 40°, (b) and (h) 60°, and (c) and (i) 75°; (d) and (j) double-pitch nanostructure showing two local maxima at 25° and 60°; (e) and (k) aperiodic nanostructures; (f) and (l) bare fiber. Left (a)–(f) and right (g)–(l) columns correspond to simulated and experimental data, respectively. Dashed lines in (a)–(d) and (g)–(j) show the local maxima angles. The color bar on the top refers to the value of the average in-coupling efficiency [from 10^{-6} (blue color) to 1 (red color) in a logarithmic scale].

previous figures—the good agreement between experiments and simulations and the improved in-coupling at large angles due to the nanostructures—are well confirmed. Among all the samples containing nanostructures, the fiber with the aperiodic nanostructure [Fig. 7(e)] clearly stands out in the context of the average in-coupling efficiency: this geometry yields a relatively high value of $\overline{\eta}_n(\theta_1, \theta_2)$ at all available angular intervals, i.e., for all combinations of θ_1 and θ_2 , which clearly underlines the relevance of employing non-periodic structures in the context of coupling light to fibers.

F. Discussion

The results presented here clearly show that sophisticated nanostructures such as aperiodic ring arrays allow improving the coupling into fibers significantly, especially at large angles, even over extended angular intervals. From our perspective, further improvement can be achieved by two approaches.

The first approach is based on the employment of more complex dielectric nanostructures such as nanoantennas or metasurfaces. It is important to mention that for the latter, significant progress has been made recently in terms of implementation via nanoprinting. For example, metasurface-based lenses composed of polymers have been realized on fibers, which achromatically focus light over the entire telecommunication range.⁸ In addition, complex-amplitude metasurfaces³⁴ composed of height-varied 3D nanopillars may be developed to flatten the angular response and further improve the in-coupling efficiency. Metasurfaces consisting of high-index materials can also be principally used, although the realization of such structures on fibers is challenging, as optical fibers have entirely different dimensions to the wafers typically used. Approaches such as modified electron-beam lithography,¹⁷ in particular with further transferring of the nanostructures to fiber¹⁰ or direct structuring of end faces¹¹ are currently being pursued, and the first promising studies have been presented. It remains to be seen whether these approaches can compete in practice with the nanoprinting process, which allows structures to be implemented on fibers in a straightforward way.

The second approach is based on using artificial intelligence for optimization of the total geometry through the engineering of the individual structural units.^{30,35} Here, for example, approaches such as particle swarm optimization or neural networks can be employed to specifically design dielectric nanostructures for a selected application. Note that the performance of the double-pitch and aperiodic structures confirms the importance of creating the on-fiber nanostructures with complex geometry.

IV. CONCLUSION

The efficient coupling of light into optical fibers is an essential requirement for many important applications. In this work, we present a promising and practically relevant concept for the tailored and efficient light in-coupling, particularly at large angles of incidence, based on the interfacing of 3D nanoprinted all-dielectric structures with optical fiber. Multiple axially symmetric structures for tailored light in-coupling have been realized on the facet of SMF-28 using direct laser writing technology, examples of which include lattices with double periodicity and aperiodic arrays. While the former allows for light coupling at two predefined angles, the aperiodicity of the latter results in an unprecedentedly high average coupling efficiency across very large angles of incidence, outperforming regular gratings and, in particular,

blank fibers by orders of magnitude. In addition to that, the axial symmetry of the implemented nanostructures brings the additional advantage that the in-coupling is independent of polarization and azimuthal angle of incidence. A particular noteworthy feature is the variation of the height of the individual elements (in addition to the in-plane structuring), representing a unique degree of freedom that comes with the nanoprinting process and being difficult to achieve with other lithographic methods. The quality of the fabricated structures and the high accuracy of the nanoprinting process are emphasized by the excellent agreement between simulation and experiment. The reached magnitude of in-coupling efficiency partially exceeds one of high-index nanostructures. The resulting all-fibers devices are highly integrated and ready-to-use directly after nanoprinting, paving the way toward a novel class of compact, flexible and practically relevant all-fiber devices with properties beyond the state-of-the-art. Applications can be found in a variety of cutting-edge fields that require highly efficient light collection over selected angular ranges, such as endoscopy or quantum technologies. In addition to optimizing in-coupling, the presented concept enables interfacing fibers with nanostructures with a substantially higher degree of complexity, including nanoantennas or metasurfaces, demonstrating a promising pathway for applying optical fibers in previously inaccessible areas of science and application.

V. METHODS

A. Numerical simulations and design strategy

Approximate parameters for the different designs have been obtained using an analytical model which is based on calculating of the overlap integral between the tangential electromagnetic field components of the transmitted plane wave and the fiber mode (here HE_{11} -mode). Numerical simulations and further optimization using the finite-element method (COMSOL Multiphysics) were performed for the design of the respective structure. First, the transmittance between two ports facing each other in a two-dimensional axial-symmetric formulation has been calculated using the wave optics module. One of the ports, the excitation port, is set to emit a TE- or TM-polarized plane wave incident on the fiber end face under the angle θ . The second port is used for the analysis and is configured as a numerical port. It simulates the field profile of the HE_{11} fiber mode as first step, and then uses this profile to calculate the coupling into this mode by evaluating the transmittance from the excitation to analyzing port. The details of both analytical and numerical models can be found in Ref. 17.

B. Sample implementation

The fiber platform relevant to this work is a SMF-28 (Corning¹) having a core and outer diameter of 8.2 and 125 μm , respectively. This commercially available step-index fiber is single-mode at the operation wavelength $\lambda = 1.55 \mu\text{m}$. The axially symmetric polymer arrays are nanoprinted onto the cleaved edge of the fibers through direct laser writing using a commercially available nanoprinting system (Photonic Professional GT2, Nanoscribe GmbH) employing a negative photore-sist resin (IP-DIP, Nanoscribe GmbH³¹). After printing, the structure was developed by a propylene glycol methyl ether acetate (PGMEA, Sigma Aldrich) and Novec 7100 (Sigma Aldrich). The refractive index data of the polymerized resin can be found in Refs. 36 and 37, yielding value of $n = 1.55$ at the operation wavelength of $\lambda = 1.55 \mu\text{m}$.³⁶ The samples were characterized by optical microscope as well as scanning electron microscope (SEM) after the actual measurements. As

examples, we show images of selected samples in Fig. 2. Positioning of the structure relative to the location of the fiber core is achieved by aligning a microscopic image of the fiber surface and the laser focus of the Nanoscribe. Here, the fiber is moved vertically and horizontally until the focus is aligned with the edge of the fiber. The related stage coordinates (x_1 , x_2 , y_1 , and y_2) are then used to calculate the center point (x_0 , y_0) corresponding to the position of the core. Note that the laser focus is visible due to the fluorescence of the resin, while operating at reduced power (e.g., 2% of maximum power) to avoid polymerization. Using this procedure, a position inaccuracy smaller than the diameter of the focus (300 nm) is expected. This assumption is confirmed by a study in which the positioning procedure was repeated multiple times, yielding a standard deviation of relative position deviation of nanostructure and fiber axis of < 4% (in relation to the diameter of the fiber core $d = 8.2 \mu\text{m}$). Note that coupling light into the free fiber end makes the core visible, defining another positioning option.

C. Setup and measurement procedure

A setup consisting of a light source and a rotatable xy -precision stage was used for the experimental determination of the coupling efficiency. For illumination, a fiber coupled superluminescent light-emitting diode (SLED) having a central wavelength of 1554 nm and a maximum power of 13 mW was used. The SLED has a 3-dB-bandwidth of 46 nm. The emitted light was collimated by a fiber collimator, resulting in a beam with a waist diameter of 0.9 mm. The light source was first polarized using a linear polarization filter, and the desired orientation of the polarization was created through rotating a half wavelength plate. To implement different in-coupling angles θ ranging from 0° to nearly 90° , the fiber under test was fixed on a xyz precision stage which was mounted on a rotation table. The fiber was oriented in such a way that its end face containing the polymer nanostructure is oriented perpendicular to the axis of rotation. Thus, the light beam always hits the polymer structure (and the fiber core) when the angle of incidence was changed. The power of the in-coupled light was measured at the opposite fiber end using an InGaAs photodiode. Before measurement, the light intensity after the lambda half plate was determined to be about $25 \text{ nW}/\mu\text{m}^2$.

SUPPLEMENTARY MATERIAL

See the [supplementary material](#) for the analysis of pitch inaccuracy impact and the detailed comparison between designed and implemented structures.

ACKNOWLEDGMENTS

We acknowledge the support of the Deutsche Forschungsgemeinschaft (DFG, German Research Foundation) under Germany's Excellence Strategy—EXC 2051 (Project-ID 390713860), and the Project Nos. SCHM2655/15–1 and SCHM2655/21–1, the Ministry of Education and Science of Ukraine (Grant No. 0122U001482), the U.S. Civilian Research and Development Foundation (CRDF Global, Grant No. G-202202–68457) and Australian Research Council (Grant No. DP210101292).

AUTHOR DECLARATIONS

Conflict of Interest

The authors have no conflicts to disclose.

Author Contributions

Oleh Yermakov: Conceptualization (equal); Data curation (equal); Formal analysis (equal); Investigation (equal); Methodology (equal); Software (equal); Validation (equal); Visualization (equal); Writing – original draft (equal); Writing – review & editing (equal). **Matthias Zeisberger:** Data curation (equal); Formal analysis (supporting); Investigation (lead); Methodology (lead); Software (supporting); Validation (equal); Visualization (supporting); Writing – review & editing (equal). **Henrik Schneidewind:** Data curation (equal); Investigation (supporting); Methodology (supporting); Validation (equal); Writing – review & editing (equal). **Jisoo Kim:** Methodology (supporting); Validation (equal); Writing – review & editing (equal). **Andrey Bogdanov:** Validation (equal); Visualization (supporting); Writing – review & editing (equal). **Yuri S. Kivshar:** Conceptualization (supporting); Validation (equal); Writing – review & editing (equal). **Markus A. Schmidt:** Conceptualization (lead); Formal analysis (supporting); Investigation (supporting); Supervision (lead); Validation (equal); Visualization (lead); Writing – original draft (equal); Writing – review & editing (equal).

DATA AVAILABILITY

The data that support the findings of this study are available from the corresponding author upon reasonable request.

REFERENCES

- ¹Corning, see <https://www.corning.com/> for “Data Sheet of Single Mode Fiber SMF-28.”
- ²M. Consales, A. Ricciardi, A. Crescitelli, E. Esposito, A. Cutolo, and A. Cusano, “Lab-on-fiber technology: Toward multifunctional optical nanoprobes,” *ACS Nano* **6**, 3163–3170 (2012).
- ³M. Pisco and A. Cusano, “Lab-on-fiber technology: A roadmap toward multifunctional plug and play platforms,” *Sensors* **20**, 4705 (2020).
- ⁴Q. Wang and L. Wang, “Lab-on-fiber: Plasmonic nano-arrays for sensing,” *Nanoscale* **12**, 7485–7499 (2020).
- ⁵Y. Xiong and F. Xu, “Multifunctional integration on optical fiber tips: Challenges and opportunities,” *Adv. Photonics* **2**, 064001 (2020).
- ⁶J. Yang, I. Ghimire, P. C. Wu, S. Gurung, C. Arndt, D. P. Tsai, and H. W. H. Lee, “Photonic crystal fiber metalens,” *Nanophotonics* **8**, 443–449 (2019).
- ⁷M. Zeisberger, H. Schneidewind, U. Hübner, T. Wieduwilt, M. Plidschun, and M. A. Schmidt, “Plasmonic metalens-enhanced single-mode fibers: A pathway toward remote light focusing,” *Adv. Photonics Res.* **2**, 2100100 (2021).
- ⁸H. Ren, J. Jang, C. Li, A. Aigner, M. Plidschun, J. Kim, J. Rho, M. A. Schmidt, and S. A. Maier, “An achromatic metafiber for focusing and imaging across the entire telecommunication range,” *Nat. Commun.* **13**, 4183 (2022).
- ⁹T. Liu, S. Yang, D. Tang, H. Da, R. Feng, T. Zhu, F. Sun, and W. Ding, “Polarization conversion based on an all-dielectric metasurface for optical fiber applications,” *J. Phys. D* **50**, 334001 (2017).
- ¹⁰C. Zhou, W.-B. Lee, S. Gao, H. Li, C.-S. Park, D.-Y. Choi, and S.-S. Lee, “All-dielectric fiber meta-tip enabling vortex generation and beam collimation for optical interconnect,” *Laser Photonics Rev.* **15**, 2000581 (2021).
- ¹¹M. Plidschun, H. Ren, J. Kim, R. Förster, S. A. Maier, and M. A. Schmidt, “Ultra-high numerical aperture meta-fiber for flexible optical trapping,” *Light* **10**, 57 (2021).
- ¹²S. Schmidt, S. Thiele, A. Toulouse, C. Bösel, T. Tiess, A. Herkommer, H. Gross, and H. Giessen, “Tailored micro-optical freeform holograms for integrated complex beam shaping,” *Optica* **7**, 1279–1286 (2020).
- ¹³G. Calafiore, A. Koshelev, T. P. Darlington, N. J. Borys, M. Melli, A. Polyakov, G. Cantarella, F. I. Allen, P. Lum, E. Wong, S. Sassolini, A. Weber-Bargioni, P. James Schuck, S. Cabrini, and K. Munechika, “Campanile near-field probes

- fabricated by nanoimprint lithography on the facet of an optical fiber,” *Sci. Rep.* **7**, 1651 (2017).
- ¹⁴M. Consales, G. Quero, S. Spaziani, M. Principe, A. Micco, V. Galdi, A. Cutolo, and A. Cusano, “Metasurface-enhanced lab-on-fiber biosensors,” *Laser Photonics Rev.* **14**, 2000180 (2020).
- ¹⁵N. Wang, M. Zeisberger, U. Hübner, and M. A. Schmidt, “Boosting light collection efficiency of optical fibers using metallic nanostructures,” *ACS Photonics* **6**, 691–698 (2019).
- ¹⁶N. Wang, M. Zeisberger, U. Hübner, and M. A. Schmidt, “Nanograting-enhanced optical fibers for visible and infrared light collection at large input angles,” *Photonics* **8**, 295 (2021).
- ¹⁷O. Yermakov, H. Schneidewind, U. Hübner, T. Wieduwilt, M. Zeisberger, A. Bogdanov, Y. Kivshar, and M. A. Schmidt, “Nanostructure-empowered efficient coupling of light into optical fibers at extraordinarily large angles,” *ACS Photonics* **7**, 2834–2841 (2020).
- ¹⁸S. Jahani and Z. Jacob, “All-dielectric metamaterials,” *Nat. Nanotechnol.* **11**, 23–36 (2016).
- ¹⁹I. Staude, T. Pertsch, and Y. S. Kivshar, “All-dielectric resonant meta-optics lightens up,” *ACS Photonics* **6**, 802–814 (2019).
- ²⁰G. Kostovski, U. Chinnasamy, S. Jayawardhana, P. R. Stoddart, and A. Mitchell, “Sub-15 nm optical fiber nanoimprint lithography: A parallel, self-aligned and portable approach,” *Adv. Mater.* **23**, 531–535 (2011).
- ²¹M. Pisco, F. Galeotti, G. Quero, G. Grisci, A. Micco, L. V. Mercaldo, P. D. Veneri, A. Cutolo, and A. Cusano, “Nanosphere lithography for optical fiber tip nanoprobings,” *Light* **6**, e16229 (2017).
- ²²V. Savinov and N. Zheludev, “High-quality metamaterial dispersive grating on the facet of an optical fiber,” *Appl. Phys. Lett.* **111**, 091106 (2017).
- ²³P. Malara, A. Crescitelli, V. D. Meo, A. Giorgini, S. Avino, E. Esposito, A. Ricciardi, A. Cusano, I. Rendina, P. D. Natale, and G. Gagliardia, “Resonant enhancement of plasmonic nanostructured fiber optic sensors,” *Sens. Actuators, B* **273**, 1587–1592 (2018).
- ²⁴N. Wang, M. Zeisberger, U. Hübner, and M. A. Schmidt, “Nanotrimer enhanced optical fiber tips implemented by electron beam lithography,” *Opt. Mater. Express* **8**, 2246–2255 (2018).
- ²⁵T. Gissibl, S. Thiele, A. Herkommer, and H. Giessen, “Sub-micrometre accurate free-form optics by three-dimensional printing on single-mode fibres,” *Nat. Commun.* **7**, 11763 (2016).
- ²⁶T. Gissibl, M. Schmid, and H. Giessen, “Spatial beam intensity shaping using phase masks on single-mode optical fibers fabricated by femtosecond direct laser writing,” *Optica* **3**, 448–451 (2016).
- ²⁷T. Gissibl, S. Thiele, A. Herkommer, and H. Giessen, “Two-photon direct laser writing of ultracompact multi-lens objectives,” *Nat. Photonics* **10**, 554–560 (2016).
- ²⁸K. Weber, F. Hütt, S. Thiele, T. Gissibl, A. Herkommer, and H. Giessen, “Single mode fiber based delivery of OAM light by 3D direct laser writing,” *Opt. Express* **25**, 19672–19679 (2017).
- ²⁹J. Li, S. Thiele, B. C. Quirk, R. W. Kirk, J. W. Verjans, E. Akers, C. A. Bursill, S. J. Nicholls, A. M. Herkommer, H. Giessen, and R. A. McLaughlin, “Ultrathin monolithic 3D printed optical coherence tomography endoscopy for preclinical and clinical use,” *Light* **9**, 124 (2020).
- ³⁰W. Hadibrata, H. Wei, S. Krishnaswamy, and K. Aydin, “Inverse design and 3D printing of a metalens on an optical fiber tip for direct laser lithography,” *Nano Lett.* **21**, 2422–2428 (2021).
- ³¹See <https://www.nanoscribe.com/> for “Nanoscribe GmbH”
- ³²M. Tanaka, K. Tanaka, and O. Fukumitsu, “Transmission and reflection of a Gaussian beam at oblique incidence on a dielectric slab,” *J. Opt. Soc. Am.* **67**, 819–825 (1977).
- ³³M. Born and E. Wolf, *Principles of Optics: Electromagnetic Theory of Propagation, Interference and Diffraction of Light* (Elsevier, 2013).
- ³⁴H. Ren, X. Fang, J. Jang, J. Bürger, J. Rho, and S. A. Maier, “Complex-amplitude metasurface-based orbital angular momentum holography in momentum space,” *Nat. Nanotechnol.* **15**, 948–955 (2020).
- ³⁵Y. Xu, X. Zhang, Y. Fu, and Y. Liu, “Interfacing photonics with artificial intelligence: An innovative design strategy for photonic structures and devices based on artificial neural networks,” *Photonics Res.* **9**, B135–B152 (2021).
- ³⁶B. Jang, J. Gargiulo, R. F. Ando, A. Lauri, S. A. Maier, and M. A. Schmidt, “Light guidance in photonic band gap guiding dual-ring light cages implemented by direct laser writing,” *Opt. Lett.* **44**, 4016–4019 (2019).
- ³⁷M. Schmid, D. Ludescher, and H. Giessen, “Optical properties of photoresists for femtosecond 3D printing: Refractive index, extinction, luminescence-dose dependence, aging, heat treatment and comparison between 1-photon and 2-photon exposure,” *Opt. Mater. Express* **9**, 4564 (2019).